Experiments in Fluids 16, 263–272 (1994)

Experiments in Fluids

Two-color particle-imaging velocimetry using a single argon-ion laser*

M. E. Post[1], D. D. Trump[1], L. P. Goss[1], R. D. Hancock[2]

[1] Systems Research Laboratories, Inc., A Division of Arvin/Calspan, 2800 Indian Ripple Road, Dayton, OH 45440-3696, USA
[2] Aero Propulsion and Power Directorate, Wright Laboratory, Wright-Patterson Air Force Base, OH 45433-7103, USA

Received: 22 October 1992 / Accepted: 22 June 1993

Abstract. A swept-beam, two-color particle-imaging velocimetry (PIV) technique has been developed which utilizes a single argon-ion laser for illuminating the seed particles in a flowfield. In previous two-color PIV techniques two pulsed lasers were employed as the different-color light sources. In the present experiment the particles in a two-dimensional shear-layer flow were illuminated using a rotating mirror to sweep the 488.0-nm (blue) and 514·5-nm (green) lines of the argon-ion laser through a test section. The blue- and green-particle positions were recorded on color film with a 35-mm camera. The unique color coding eliminates the directional ambiguities associated with single-color techniques because the order in which the particle images are produced is known. Analysis of these two-color PIV images involved digitizing the exposed film to obtain the blue and green-particle image fields and processing the digitized images with velocity-displacement software. Argon-ion lasers are available in many laboratories; with the addition of a rotating mirror and a few optical components, it is possible to conduct flow-visualization experiments and make quantitative velocity measurements in many flow facilities.

List of symbols

d	length of displacement vector
d_m	distance between rotating mirror and concave mirror
n_f	number of facets on rotating mirror
R	seed-particle radius
v	velocity in x, y plane
v_s	sweep velocity of laser beams, assumed to be in y direction from top to bottom of field of view
v_x, v_y, v_z	x, y, and z components of velocity
x_1, y_1	color-1 particle coordinates
x_2, y_2	color-2 particle coordinates
y_{max}	y dimension of field of view, assumed to be the long dimension
Δs	spatial separation of beams as they approach rotating mirror
Δt	time separation of laser sheets or of swept beams passing fixed point
Δt_b	time between successive sweeps through test section by same beam
Δt_s	time required for both beams to sweep through test section
$\Delta\theta$	angular separation of beams reflecting from rotating mirror
μ	fluid viscosity
ν	angular velocity of rotating mirror in cycles per second
ρ	seed-particle density
τ	seed-particle response time
$\sigma_v, \sigma_d, \sigma_t$	standard deviation of velocity, displacement, and time
ω	vorticity

1 Introduction

In the characterization of complex flows (e.g., recirculating), it is advantageous to obtain an instantaneous picture of the entire flowfield rather than a time-averaged pointwise map. The global view resulting from instantaneous two-dimensional measurements can provide insight into spatial correlations of systems such as unsteady or cyclical flows where interpretation of time-averaged pointwise data may be difficult.

Several techniques which can be used to determine the two-dimensional velocity of a flowfield have been reported in the literature; these include: PIV methods based on the correlation of particle displacements (Meynart 1980, 1983, Yao and Adrian 1984, Adrian and Yao 1985, Adrian 1986, Landreth et al. 1986, Coupland et al. 1987, and Ruess et al. 1989), time-of-flight techniques (Hiller et al. 1984, Miles et al. 1989, and Boedeker 1989) and planar-laser-induced-fluorescence (PLIF) methods (Hiller et al. 1983, McDaniel et al. 1983, Hiller and Hanson 1985, 1988). For low-to-moderate velocity flowfields, particle-displacement techniques such as particle-imaging velocimetry (PIV) are effective and offer a wide velocity-measurement range. The PIV technique involves 1) double pulsing a particle-laden flowfield, 2) photographing the light scattered by the particles and 3) processing the photographs to obtain velocity information.

The principle of two-color PIV was suggested by Adrian (1986) and first implemented by Goss et al. (1989). This technique provides a means of removing the directional ambiguities associated with double-pulsed,

* This work was supported, in part, by the Aero Propulsion and Power Directorate of Wright Laboratory under Contract No. F33615-90-C-2033.

Correspondence to: M. E. Post

one-color PIV methods because the order in which the particle images are produced is known. In the pulsed-laser sheet-lighting mode of two-color PIV, seed particles are illuminated with a light sheet (Color-1) produced by passing the output from a pulsed laser through a cylindrical lens. After a selected time interval (ranging from a few microseconds to milliseconds for high- and low-velocity flow systems, respectively), a co-planar light sheet (Color-2) from a second pulsed laser is used to illuminate the particles. Particles which remain in the plane of the laser sheets produce a "displacement-vector" pair comprised of a Color-1 and a Color-2 particle image. The Mie scattering from the seed particles is recorded on color film and processed by direct digitization. This mode of PIV has been utilized to measure two-dimensional flowfields in a turbine-cascade test section with velocities ranging from 50 to 340 m/s (Goss et al. 1989) and in a propane diffusion flame with velocities ranging from 0 to 3 m/s (Goss et al. 1991).

In most PIV applications, correlation analysis is used to find the average displacement of particle pairs within the correlation region. High seed densities provide many pairs in a small region. This results in high spatial resolution and a statistically accurate average of the particle displacement. If the seed density is in a lower range, it is possible to match individual particle pairs (particle tracking) using correlation analysis to guide the particle-tracking algorithm. The modified correlation technique employed in this study utilizes particle-coordinate information rather than intensity information and requires fewer operations than standard correlation methods; the dimensions of the correlation region are limited neither by optical constraints nor by size constraints associated with digital FFT algorithms.

The pulsed-laser sheet-lighting mode of operation has been used for most one- and two-color PIV measurements. The exceptions are Kawahashi and Hosoi (1989, 1991) and Gray et al. (1991) who used the continuous output of an argon-ion laser to perform one-color PIV in a swept-beam mode. For the experiments described in the present paper, the swept-beam concept was extended to two-color PIV by making use of the fact that the argonion laser has several distinct lines which can be separated and swept through the sample volume in a selected order.

2 Theory

2.1 Velocity calculation

The basic principle of PIV is straightforward – the average velocity of a two-color particle-image pair is determined by dividing the vector displacement by the time increment between pulses

$$(v_x, v_y) = (x_2 - x_1, y_2 - y_1)/\Delta t \tag{1}$$

where (x_1, y_1) and (x_2, y_2) are the positions of the particles when illuminated by Color-1 (first) and Color-2 (second) light sources, respectively. An overview of the methods used to find average displacement and track individual particle pairs is presented in Sect. 2.4 (image analysis).

In previous two-color PIV experiments in this laboratory, the seed particles were illuminated by successive light sheets, and all particles in the test region were imaged simultaneously for each color. In swept-beam experiments a correction is required to account for the fact that all particles are not illuminated simultaneously. When the beams sweep through the test section in an orientation perpendicular to the vertical dimension, the separation between the Color-1 and Color-2 images of a seed particle is given by

$$x_2 - x_1 = v_x(\Delta t)\frac{v_s}{v_y + v_s} \tag{2}$$

$$y_2 - y_1 = v_y(\Delta t)\frac{v_s}{v_y + v_s} \tag{3}$$

where Δt is the time interval between the Color-1 and Color-2 beams entering the test section, v_s is the "sweep" velocity of the beams as they pass through the test section, and the sweep direction is assumed to be the y direction (thus, the denominator of each term contains v_y). As the sweep velocity increases, the velocity ratio in Eqs. (2) and (3) approaches unity, and these expressions for particle displacement approach those which would be obtained using Eq. (1).

2.2 Light scattering

The amount of light scattered by a particle is a function of the particle size and shape, the wavelength of the laser beam, and the intensity of the light incident on the particle. The detection of the scattered light is dependent upon the collection optics and the scattering angles. As particle size decreases, the energy density of the light beam must be increased to produce sufficient scattered light for imaging the particle. These issues are treated by Adrian and Yao (1985), Goss et al. (1989), and Smallwood (1992). With the swept-beam PIV technique, the laser beam retains its high-energy density because it is not formed into a sheet. This makes possible the imaging of small particles with a source that might have insufficient energy density if it were spread into a light sheet.

2.3 Particle flow response

The ability of the seed particles to follow the flowfield is dependent upon the size, density, and shape of the particle and the viscosity, density, and speed of the fluid. For

low-velocity flows the response time of a spherical particle is given by

$$\tau = \frac{2R^2\rho}{9\mu} \tag{4}$$

where R is the particle radius, ρ is the particle density, and μ is the fluid viscosity. Hollow microballoons (phenolic resin) were used to seed the flow in this study; their low density decreases their response time, enabling them to follow the fluid flow more closely than solid particles of the same size. The large surface area of the microballoon also makes it more effective as a light scatterer. As the ratio of the particle response time to the characteristic time of changes in the flow decreases, particles can follow the flow more closely.

2.4 Image analysis

The analysis procedure consists of 1) determining the spatial locations of the particle images, 2) constructing a correlation map from which the average displacement vector can be determined, and 3) utilizing this information in a tracker which locates vectors between particle-image pairs.

The color negatives were digitized with a high-resolution (4096×6144 pixels) color scanner. This produces a separate digital image for each emulsion layer of the film. In this experiment the blue and green emulsion layers were utilized. An important factor in the success of this analysis is that the "cross-talk" between emulsion layers must be minimized. This minimization is dependent on the spectral sensitivity of the film, the intensity of the scattered light, and the transmission characteristics of the scanner. These issues have been reviewed by Smallwood (1992).

The digitized images are processed to find the particle locations. In this study particle-location information is used to perform a modified correlation analysis and to match particle-image pairs. Particle-location information makes it possible to reduce substantially the number of operations in the correlation analysis, to identify regions where no particles are present (no correlation is possible), and to eliminate intensity weighting. The disadvantages associated with finding particle locations are that the process is somewhat subjective in nature and may be relatively slow.

The parameters used to identify particles are minimum radius, maximum radius, and intensity threshold. The values of these parameters are somewhat subjective, and it is possible to select values that identify only those particles that are clearly evident from a visual inspection of the photograph or values that identify nearly every local intensity maximum as a particle. Minimum and maximum radius parameters can be estimated with reasonable accuracy by examining the photograph. A useful intensity criterion is to identify particles having an intensity that is one standard deviation above the average intensity of all local intensity maxima that satisfy the size criteria. In practice this procedure tends to identify some local noise peaks as particles, but, in general, the correlation methods are effective, even in cases where some random noise is present. If the number of particles identified by this process is found to be too large or too small, the intensity criterion can be altered using some multiple of the standard deviation to modify the threshold intensity.

Since light-scattering properties are dependent on particle diameter, a range of particle diameters has the potential to introduce complexity into the particle-finding process. When the imaging system is optimized for a given particle size, smaller particles may not scatter sufficient light to expose the film, while larger particles may saturate the film (with the possibility of exposing both the blue and the green layers of film emulsion at the same time). If all particles were overexposed and imaged in both the blue and the green emulsion layers, the data obtained would be equivalent to that obtained in a one-color, double-pulsed experiment. The experimental approach in the present study was to vary the laser intensity, magnification, $f\#$, and film speed to determine operating values which would minimize the amount of "cross-talk" between the layers of film emulsion.

After the particles have been identified, the images are divided into sub-sections and a modified cross-correlation method used to obtain an estimate of the average particle displacement within each subsection. The average displacement is identified as the location of the maximum in the correlation map. The base of each displacement vector is assigned to the center of the subsection used to construct the correlation map.

The particle-tracking algorithm is based on the interpolation of the average displacements. The location of a Color-1 (blue) particle is identified, and the average displacements for the image subsection are interpolated to obtain a local estimate of the displacement of the blue particle. The estimated displacement is added to the position of the blue particle to obtain a "target" location for a Color-2 (green) particle. A search of the green particle locations is made to find a green particle within a specified uncertainty of the "target" position. If a green particle can be found which satisfies this criterion, it is accepted as the match. The overall number density of green particles should be such that the probability of making a random match is low. The criterion used in this study was that the number of particles per unit area times the area of the uncertainty in the "target" position must be less than 0.1. This criterion is arbitrary and corresponds roughly to a requirement that no more than 10% of the matches can be due to random effects. These procedures have been

discussed in more detail by Goss et al. (1989) and Post (1994).

3 Experimental

3.1 System components

The experimental arrangement for swept-beam, two-color PIV measurements is shown in Fig. 1. The output of a multiple-line argon-ion laser was separated into its individual components using a dispersion prism, and the 488.0-nm (blue) and 514.5-nm (green) laser lines were employed to sweep the test section. The laser was operated at ~1.5 W (all lines). The power of the blue beam was ~0.5 W and that of the green beam was ~0.6 W; the remaining power was distributed among the other beams produced by the laser. The beams were directed to a rotating mirror (10 facets, axis rotating at 25 Hz), swept across a concave mirror (15-cm diameter, 75-cm focal length), and reflected through the test section one after the other. The concave mirror was used to orient the scanning beams perpendicular to the major flow axis of the test section. A PIN diode was employed to detect the beams as they passed through the test section, and a time delay of 2.0 ms between beams was measured by viewing the output of the diode on an oscilloscope. In the present study the sweep velocity was 220 m/s, and the maximum v_y value was about 1 m/s. For this case the error introduced by neglecting the velocity ratio in Eqs. (2) and (3) is $<0.5\%$.

For the shear-layer flow, the experimental arrangement (Fig. 2) consisted of a square duct (12.7 cm on a side), with a splitter plate dividing the inlet into two equal sections. The air velocity was 0.94 m/s on the high-speed side and 0.47 m/s on the low-speed side (based on volume flow rates and cross-sectional areas). This setup is being used as part of a study of the interaction of droplets with the large coherent structures produced by the shear-layer flow. The swept-beam two-color PIV technique was employed to measure the two-dimensional velocity profile of the shear-layer flow prior to introduction of droplets into the system. The flow was driven at 30 Hz with a loud speaker placed in the air-supply line for the low-velocity side of the flow. The seed – phenolic microballoons (UCAR Phenolic Resin, Union Carbide) of 100-μm nominal diameter (range 5–200 μm) – was injected into both flow channels upstream of the splitter plate. The microballoons have an average wall thickness of about 1 μm and an average density of 0.104 gm/cm^3. The response time of the microballoons in room-temperature air was calculated to be 2.91 ms [Eq. (4)]. The characteristic time based on the average shear-layer thickness (6.3 mm) divided by the velocity difference across the shear layer (0.47 m/s) is 13.4 ms.

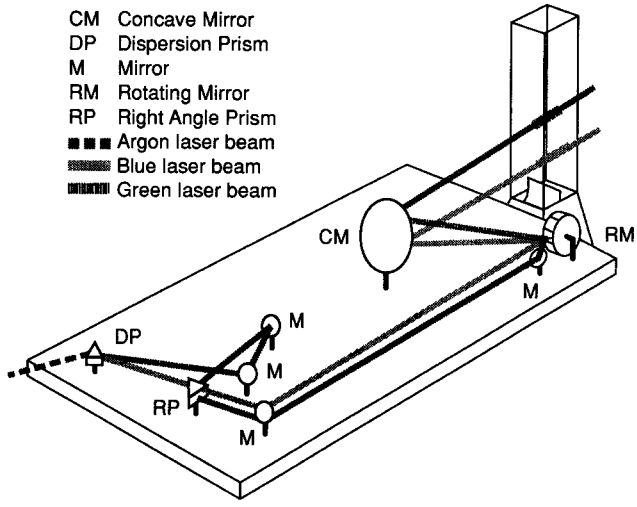

Fig. 1. Experimental arrangement for swept-beam two-color PIV technique

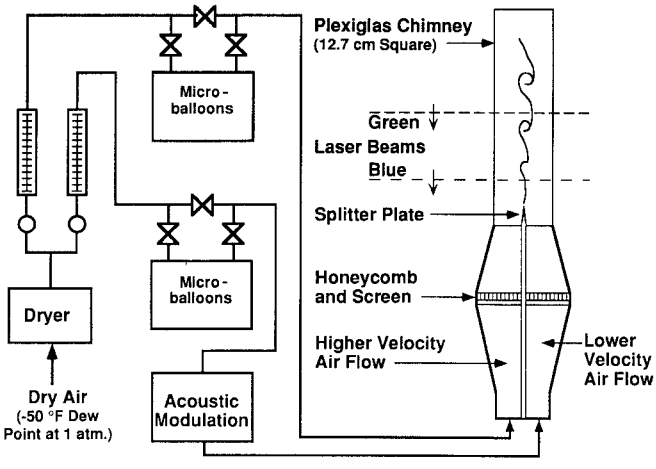

Fig. 2. Schematic diagram of splitter-plate test facility

A 35-mm Nikon camera with an exposure time of 1/250 s was employed to record the Mie scattering of the particles in the seeded flowfield. Photographs were taken using a focal-plane shuttered camera with a 50-mm lens, and the camera aperture was set at *f*/2.6. The magnification factor was 0.15. Kodak Gold-400 color film was used to record the two-color PIV images, and the film was processed commercially.

The success of any PIV experiment depends upon the care with which the optical components of the system are aligned. The beams must be co-planar as they sweep through the test section; otherwise, the two color images obtained will be of particles in different planes. The windows of the test section should be oriented perpendicular to the laser beams in such a way that reflections within the

test section will be in the same plane as the swept beams. Otherwise, a set of ghost images of particles will be produced in a different plane. These images introduce noise into the PIV photograph and interface with analysis of the data. Finally, the camera should be oriented perpendicular to the plane of the swept beams.

The relationship between distance in the plane of the swept beams and digitized pixels in the actual PIV picture was determined by photographing a scale. The plane of the scale was placed at an angle to the plane of the swept beams that facilitated visualization of the edge of the sweep plane. The length-per-pixel factor (39.2 μm/pixel) was calculated by dividing the length of the scale by the number of pixels used to digitize that length. The scale photograph was also used to verify that the sweep plane of the laser beams was in the center of the depth of field and to estimate the beam width (less than 1 mm) in the sweep plane.

3.2 Timing

Application of swept-beam two-color PIV techniques to other experiments requires adjustment of several time intervals and synchronization of a number of events. The time intervals involved are 1) the time separation of the swept beams, 2) the time required for one sweep of the entire test section by both beams, 3) the time separation of successive sweeps by the same beam, and 4) the time required for illumination of a single particle. The most important synchronization event involves opening the camera shutter while the beams are sweeping through the test section; it may also be necessary to synchronize the camera shutter and swept beams with a transient or cyclical event.

The relevant time intervals are dependent upon the speed (v_s) at which the beams are swept across the concave mirror surface and through the test section

$$v_s = 4\pi d_m \nu \tag{5}$$

where d_m is the distance between the rotating and the concave mirrors and ν is the angular velocity of the rotating mirror in cycles for per second (4π is the usual 2π factor for axial rotation multiplied by 2 for the reflection from the plane mirror surfaces of the rotating mirror). The sweep speed should be set at a value which is high compared to the maximum expected velocity in the experimental system in order that the velocity ratio in Eqs. (2) and (3) will approach unity.

The first time interval (Δt) of interest is that between the swept beams. This interval can be adjusted by two methods. First, for parallel beams the spatial separation (Δs) results in a temporal separation (Δt) since the rotating-mirror face causes the Color-1 (blue) beam to reach the edge of the concave mirror before the Color-2 (green) beam. As Δs is increased, Δt increases; however, Δs is limited, in practice, by the size of the faces of the rotating mirror. For the case where the beams are parallel, Δt is calculated using

$$\Delta t = \frac{\Delta s}{v_s} = \frac{\Delta s}{4\pi d_m \nu} \tag{6}$$

The range of Δt values can also be adjusted by changing the angle ($\Delta\theta$) between the swept beams as they are reflected from the rotating-mirror surface. For this case, Δt is calculated using

$$\Delta t = \frac{\Delta\theta}{4\pi\nu} \tag{7}$$

In either case, the time delay is measured from the output of a PIN diode on an oscilloscope.

The product of Δt and the expected velocity is the expected particle displacement. The maximum expected displacement is of the same order as the minimum spatial resolution; thus, it is desirable to decrease this displacement by decreasing Δt. As the displacement decreases, the relative error in measuring the displacement increases. The trade-off between these two factors must be considered when selecting the value of Δt.

The second time interval (Δt_s) of interest is that required for both beams to sweep the test section. The camera shutter must be open for at least this amount of time to permit illumination of the full test section with both beams. This interval is calculated using

$$\Delta t_s = \frac{y_{\max}}{v_s} + \Delta t \tag{8}$$

where $y_{\max}$ is the dimension of the field of view perpendicular to the sweep direction. Note that as v_s increases, Δt_s approaches Δt.

The third time interval (Δt_b) of interest is that between successive sweeps of the same beam. The camera shutter must be open for a time period which is shorter than this interval; otherwise, a portion of the test section will be illuminated twice by successive scans of the same beam. This interval is inversely proportional to the product of the angular velocity of the rotating mirror, ν, and the number of facets on the mirror, n_f. For a multi-faceted mirror of the type used in this experiment, this product can be adjusted by altering the angular velocity of the mirror or by changing the number of facets on the mirror, e.g., by blackening facets with paint or tape. This time interval is calculated using

$$\Delta t_b = \frac{1}{\nu n_f} \tag{9}$$

The fourth time interval of interest is that required for illumination of a single particle. This interval should not be confused with the time period during which the camera shutter is open. The shutter may be open for a relatively

long time, but the particles are illuminated for a very short time. In the pulsed-laser sheet-light mode of two-color PIV, all particles in the field of view are illuminated for a time equal to the pulse length (about 10 ns). In the swept-beam mode, individual particles are imaged in a time which is equal to the beam diameter divided by v_s (assuming the particle diameter to be much smaller than the beam diameter and the sweep velocity to be much higher than the particle velocity). For the sweep speed of 220 m/s and the beam diameter of 1.0 mm in this experiment, the illumination time was 4.55 μs. The maximum expected velocity was 1.0 m/s; thus, the particles moved a maximum distance of 4.55 μm while being illuminated. This distance represents only a fraction of a pixel in the digitized image and was negligible in comparison to the maximum expected displacement of 51 pixels.

The most important synchronization event involves opening the camera shutter while the beams are sweeping through the test section; this can be accomplished by placing a color filter in front of a photodiode to detect the approach of one of the beams. Adjustment of a time delay triggers the camera shutter to open as the first beam enters the test section. It is also possible to operate in an asynchronous mode where the camera shutter is opened at random for a time longer than required for both beams to sweep the test section but shorter than that between successive sweeps by the same beam; however, in this mode some of the PIV photographs will not be useful. If synchronization with transient or cyclical events is necessary, customized electronics and detectors are required.

In the present study the sweep velocity and the required time intervals discussed above were calculated as follows. Equation (5) was used to calculate a sweep velocity of 220 m/s (for a 10-facet rotating mirror operating at an angular velocity of 25 Hz with a distance of 70 cm between the rotating and the concave mirrors). This value met the criterion that the sweep velocity must be much higher than the maximum expected flow velocity which was 1.0 m/s. A maximum displacement of 2.0 mm was chosen for a blue/green-particle pair. This distance was small compared to characteristic dimensions of changes in the flowfield but sufficiently large to have an equivalent length of 51 pixels in the digitized image. A 1-pixel error in this length would result in a relative error of 2.0%. The required time separation of the swept beams (2.0 ms) was calculated by dividing the maximum particle displacement by the maximum expected velocity. Equation (7) was used to calculate the 36-deg. angular separation of the beams as they were reflected from the rotating mirror. Equations (8) and (9), respectively, were used to calculate the minimum (3.4 ms) and maximum (4.0 ms) times during which the camera shutter would be open.

3.3 Accuracy and resolution

The accuracy of an individual velocity measurement is dependent upon the accuracy with which the time interval between the two swept beams is measured and the position of the two particle centers is determined. Wernet and Edwards (1990) used the following expression to estimate the error in a velocity measurement

$$\frac{\sigma_v}{v} = \sqrt{\left(\frac{\sigma_d}{\Delta d}\right)^2 + \left(\frac{\sigma_t}{\Delta t}\right)^2} \tag{10}$$

where v, d, and t are the velocity, displacement, and time, respectively. In the present study the positions of the first- and second-color images were determined to within 0.5 pixels; thus, the displacement is accurate to within 0.7 pixels, and the relative error is on the order of 0.7 pixels divided by the displacement in pixels. The relative error increases as the particle displacement decreases. The time interval between pulses is measured with an oscilloscope to within 2%. This uncertainty could be reduced through the use of a digital electronic counter and a fast-response diode.

The incremental velocity change (0.0196 m/s) associated with a displacement of 1 pixel was determined by dividing the equivalent length of a single pixel (39.2 μm) by the time separation between laser pulses (2.0 ms). The 0.7-pixel uncertainty in particle displacement corresponds to an absolute error on the order of 0.0139 m/s.

The uncertainty of the displacement for a matched pair is 0.7 pixels. For interpolated values of displacement, the uncertainty is a function of the weighting factors used in the interpolation and the uncertainties of the values being interpolated. Since the sum of the weighting factors is unity and the uncertainty in the individual displacements is 0.7 pixels, the uncertainty in the interpolated displacements is also on the order of 0.7 pixels.

In one-color PIV the diffraction-limited particle image size represents the lowest resolvable distance between images of a particle since no two images of a particle can be resolved closer than their diameters. This problem can be eliminated by shifting the second-pulse images relative to the first-pulse images. Adrian (1986) discussed methods (including color) for accomplishing this and has successfully implemented a shifting-mirror technique and a polarization technique. In two-color PIV the particles are imaged in different layers of the color-film emulsion. In image-shifted PIV methods, the uncertainty in measuring average displacements is the sum of the uncertainty in finding the center of the peak in the correlation map and the uncertainty in the shift. For two-color methods the shift is zero.

The maximum resolvable displacement is one-half the dimension of the correlation region. In practice, it is difficult to measure displacements that have a peak on the

edge of the correlation map, and a practical limit of 0.4 times the dimension of the correlation region was used in this study.

The average particle displacements were obtained by performing a correlation analysis of subsections of the data. The size of the correlation regions is the spatial distance over which the data are averaged, and the average displacements cannot resolve changes over shorter distances. The lower limits of the correlation scale are set, in practice, by the seed-particle density since a sufficient number of particles must be included within the subsection to render the correlation meaningful.

3.4 Alternative experimental configuration

An alternative experimental configuration would involve separation of the two different-color beams from the argon-ion laser, use of Bragg cells to pulse the beams, and direction of the pulsed outputs through sheet-forming optics. This configuration is similar to the pulsed-laser sheet-light mode of operation. At the low power levels available for the present study (argon-ion laser operating at 1.5 W), the energy density in the light sheets would have been insufficient for production of adequate PIV photographs. It may be possible to achieve success in this configuration with a laser operating at higher power levels, but the average power for CW lasers is generally lower than the instantaneous pulse power available from pulsed lasers. It may also be possible to maintain a high energy density by restricting the light sheets to a smaller area and focusing on a smaller field of view. In the present study the laser lines were selected because of their relatively high power.

4 Results and discussion

Swept-beam two-color PIV was demonstrated in this study by measuring the two-dimensional velocity field above the trailing edge of a splitter plate. An image of the flow is visualized using the Reactive Mie Scattering (RMS) technique (Chen and Roquemore 1986) is shown in Fig. 3. This image, collected under the same flow conditions as the PIV photograph, shows the interface between the two fluids and is included to give the reader a view of the vortex structures. Two-color PIV photographs have been omitted because they do not reproduce well in black and white. The PIV photograph was digitized and particle-finding software used to locate the positions of the blue- and green-particle centers (Fig. 4a). In this case 2543 blue particles and 2381 green particles were located. Not every blue-particle image has a matching green-particle image in this data set since out-of-plane components of the velocity transport particles out of the field of view. If the beams are perfectly aligned, $1-(v_z \Delta t/w)$ represents the

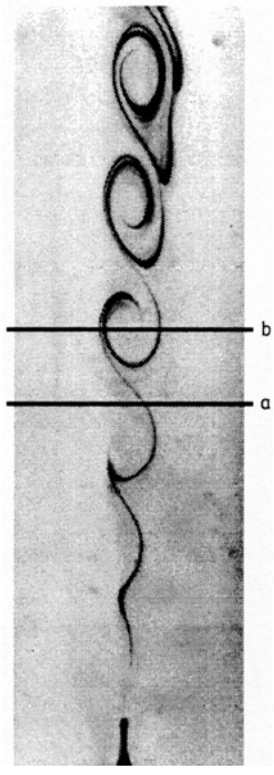

Fig. 3. Visualization of shear layer by reactive Mie scattering. Flow conditions and driving frequency are same as for PIV experiment. Line *a* marks position between vortex structures; line *b* marks position through vortex center

fraction of blue particles which have a matching green particle (v_z is the out-of-plane velocity component, and w is the light-sheet thickness). Differences in beam diameters and sweep-plane locations as well as the efficiency of the particle-finding algorithm must also be considered. The maximum number of matches possible is the number of blue or green particles, whichever is lower.

The particle-center coordinates were grouped into sections and analyzed with correlation techniques. The number of matches totaled 896, which represents 38% of the number of matches possible if all 2381 green particles had been matched. The displacement-vector pairs are shown in Fig. 4b. The origin of the velocity vectors is the position of the blue particles. The length and direction of the vectors are directly proportional to the particle velocities. The velocity vectors (obtained by dividing the displacement by the time interval between laser pulses) are tangent to the streamlines of the flow at the instant when the photograph was taken. In Fig. 4 the direction of the flow is upward, with high speed on the left and low speed on the right. For the digitized image resolution of 39.2 μm/pixel and a time separation of 2.0 ms between beams, a single pixel in a displacement vector represents 0.0196 m/s. The tip of the splitter plate is at pixel coordinates $x=950$, $y=50$, and the field of view is 6.7×15.7 cm.

A three-point, inverse-distance algorithm was used to calculate an interpolated velocity field on a two-dimensional grid for graphical representations of the data

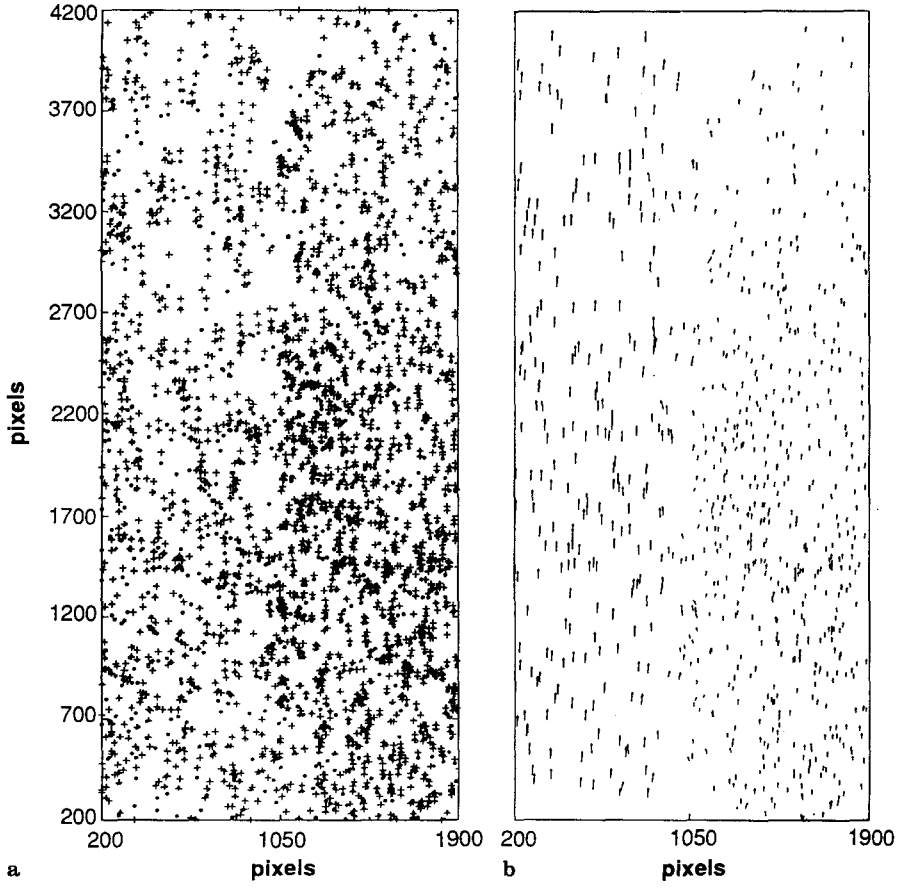

Fig. 4. a Blue- and green-particle coordinates obtained from PIV image; **b** displacement vectors between matched blue/green pairs obtained from PIV image

with contour plotting software. The interpolated velocity field was employed to calculate the magnitude of the velocity using

$$v=\sqrt{v_x^2+v_y^2} \tag{11}$$

The velocity contours in Fig. 5a show the expected gradient between the high- and low-velocity sides of the shear layer.

Figure 6 is a plot of velocity as a function of x for two values of y – one through the vortex center at $y=1800$ (6.9 cm above the splitter plate) and one between the vortex structures at $y=1500$ (5.7 cm above the splitter plate). Outside the shear layer the average velocity was 1.01 m/s on the high-speed side and 0.47 m/s on the low-speed side. These values compare favourably with those of 0.94 m/s and 0.47 m/s calculated from volume flow rates and cross-sectional areas. The measured velocity difference across the shear layer was 0.54 m/s.

The vorticity is calculated from the interpolated velocity field using

$$\omega=\frac{\Delta v_x}{\Delta y}-\frac{\Delta v_y}{\Delta x} \tag{12}$$

The vorticity contours in Fig. 5b show the location of the vortex structures. The magnitude of the vorticity at the

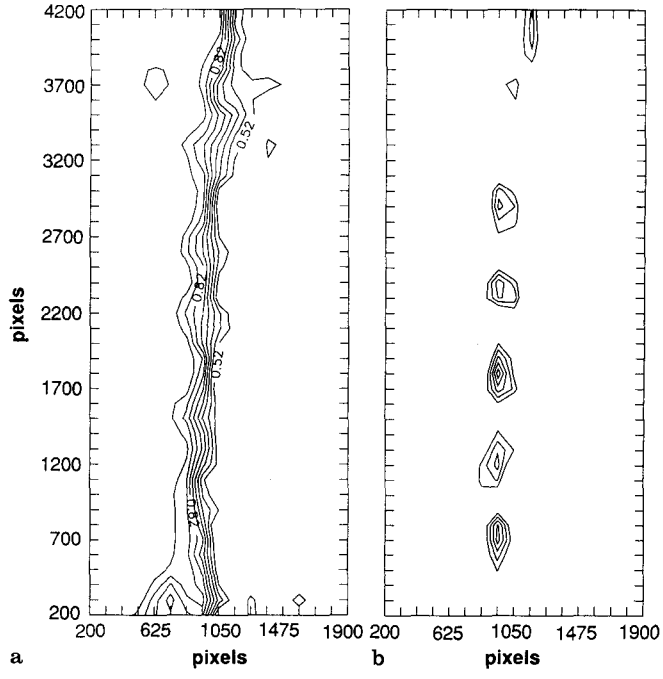

Fig. 5. a Shear-layer velocity contours from interpolated PIV data **b** shear-layer vorticity contours from interpolated PIV data

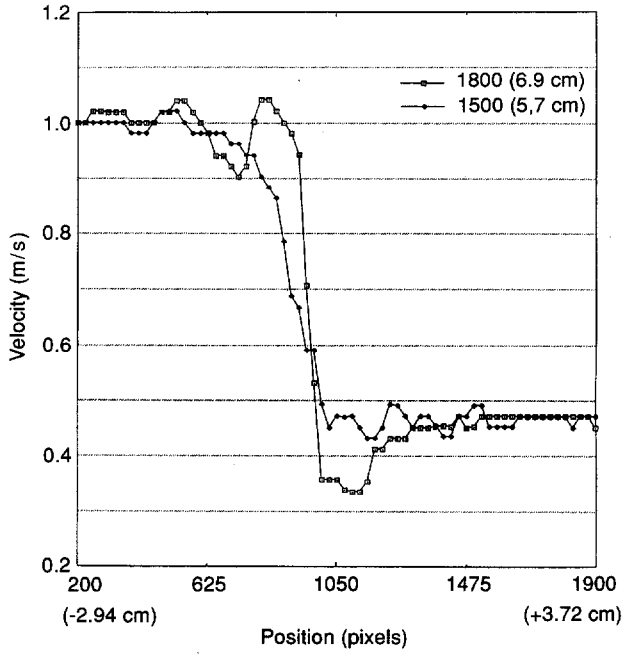

Fig. 6. Velocity profiles at $y=1500$ pixels and $y=1800$ pixels from interpolated PIV data. $y=1500$ pixels was between vortex structures, 5.7 cm above splitter plate. $y=1800$ pixels profile was through vortex center, 6.9 cm above splitter plate

vortex centers was on the order of 250 s^{-1}. The spacing between the vortex centers was estimated to be about 550 pixels (21.6 mm).

A comparison of Figs. 4 and 5 indicates that fewer particles are present in the vortex centers than in the region surrounding the vortices. Fewer vector matches are identified in areas where the particle number density is low. One reason for this is that the particles are too large to follow the flow near the vortex center. It may be possible to improve this situation through the use of smaller seed particles.

A comparison of Figs. 5a and 5b reveals that the locations of the vortex structures correspond to the steepest velocity gradients. This may seem contrary to intuition, based upon the flow visualization in Fig. 3. A steep velocity gradient would usually be inferred along Line *a* where a distinct boundary is present between the high- and low-speed fluids; a more gradual velocity gradient would be inferred along Line *b* where the boundary between fluids is stretched and wrapped into its characteristic spiral shape. The PIV data (Fig. 5) indicate that this is not the case and show that the steeper velocity gradient does, in fact, pass through the vortex. Katta (1992) has used CFD methods to model shear-layer flow under conditions very similar to those in this study. The CFD and PIV data exhibit similar behavior (i.e., steeper velocity gradients through vortex centers and more gradual gradients between vortex structures).

The relative steepness of the velocity gradients through a vortex center and between vortex structures was measured by determining the positions where the velocity reached values of 10% and 90% of the difference across the shear layer for the profiles in Fig. 6. The corresponding speeds were 0.524 and 0.956 m/s, respectively. The width of this layer through the vortex center ($y=1800$ pixels, 6.9 cm above splitter plate) was 2.4 mm and between the vortex structures ($y=1500$ pixels, 5.7 cm above splitter plate) was 10.2 mm. As noted above, the spacing between vortex centers (vortex diameter) is about 22 mm (550 pixels). The width of the velocity layer through the vortex center is significantly less than might be inferred based upon the size of structures visualized in Fig. 3. The average shear rate at the location $y=1800$ pixels was 180 s^{-1} and that at $y=1500$ pixels was 42 s^{-1}.

The apparent differences between the velocity field inferred from the visualization data (Fig. 3) and the velocity contours (Fig. 5) calculated from PIV data are attributed to the fact that the visualization data reveal the location of particles produced by reaction of trace components in the high and low-speed fluids. The concentration and location of these particles are influenced by the underlying velocity field, but the particle positions do not directly reveal the velocity magnitudes or gradients.

5 Summary

A new swept-beam two-color PIV technique has been developed which utilizes a single argon-ion laser to illuminate the particles in a seeded flowfield. Two-color PIV has the advantage that direction as well as particle displacement is uniquely determined because the first-color particle image occurs before the second-color one by a known time increment. The technique is applicable to complex flows (e.g., recirculating), where the normal 180° directional ambiguity of single-color techniques can be troublesome. An advantage of swept-beam PIV is that a single laser is used to produce the different-color laser beams, rather than two pulsed lasers. Argon-ion lasers are available in many laboratories; with the addition of a rotating mirror and a few optical components, it is possible to conduct flow-visualization experiments and make quantitative velocity measurements in many flow facilities.

Acknowledgements

The authors are indebted to Dr. W. M. Roquemore for support and discussions concerning this work and to M. Whitaker for editorial assistance and preparation of the manuscript.

References

Adrian, R. J. 1986: Image shifting technique to resolve directional ambiguity in double-pulsed velocimetry. Appl. Opt. 25, 3855–3858

Adrian, R. J.; Yao, C. S. 1985: Pulsed laser technique application to liquid and gaseous flows and the scattering power of seed materials. Appl. Opt. 24, 44–52

Boedeker, L. R. 1989: Velocity measurement by H_2O photolysis and laser-induced fluorescence of OH. Opt. Lett. 14, 473–475

Chen, L. D.; Roquemore. W. M. 1986: Visualization of Jet Flames. Combust. Flame 66, 81–86

Coupland, J. M.; Pickering, C. J. D.; Halliwell, N. A. 1987: Particle image velocimetry: theory of directional ambiguity removal using holographic image separation. Appl. Opt. 26, 1576–1578

Goss, L. P.; Post, M. E.; Trump, D. D.; Sarka, B.; MacArthur, C. D.; Dunning, G. E. Jr. 1989: A novel technique for blade-to-blade measurements in a turbine cascade. AIAA-89-2691

Goss, L. P.; Post, M. E.; Trump, D. D.; Sarka, B. 1991: Two-color particle-imaging velocimetry. J. Laser Appl. 3, 36–42

Gray, C.; Greated, C. A.; McCluskey, D. R.; Easson, W. J. 1991: An analysis of the scanning beam PIV illumination system. Meas. Sci. Technol. 2, 717–724

Hiller, B.; Booman, R. A.; Hassa, C.; Hanson, R. K. 1984: Velocity visualization in gas flows using laser-induced phosphorescence of biacetyl. Rev. Sci. Instrum. 55, 1964–1967

Hiller, B.; Hanson, R. K. 1985: Two-frequency laser-induced fluorescence technique for rapid velocity-field measurements in gas flows. Opt. Lett. 10, 206–208

Hiller, B.; Hanson, R. K. 1988: Simultaneous planar measurements of velocity and pressure fields in gas flows using laser-induced fluorescence. Appl. Opt. 27, 33–48

Hiller, B. J.; McDaniel, J. C.; Rea, E. C.; Jr Hanson, R. K. 1983: Laser-induced fluorescence technique for velocity field measurements in subsonic gas flows. Opt. Lett. 8, 474–476

Katta, V. R. 1992: Systems Research Laboratories, Inc., Dayton, Ohio, Private communication

Kawahashi, M.; Hosoi, K. 1989: Beam-sweep laser speckle velocimetry. Exp. Fluids 8, 109–111

Kawahashi, M.; Hosoi, K. 1991: Dual-beam-sweep laser speckle velocimetry. Exp. Fluids 11, 278–280

Landreth, C. C.; Adrian, R. J.; Yao, C. S. 1986: Double-pulsed particle image velocimetry with directional resolution for complex flows. Tenth Biennial Symposium on Turbulence, Rolla, Missouri, 1986

McDaniel, J. C.; Hiller, B.; Hanson, R. K. 1983: Simultaneous multiple-point velocity measurements using laser-induced iodine fluorescence, Opt. Lett. 8, 51–53

Meynart, R. 1980: Equal velocity fringes in a Rayleigh-Bernard flow by a speckle method. Appl. Opt. 19, 1385–1386

Meynart, R. 1983: Instantaneous velocity field measurements in unsteady gas flow by speckle velocimetry. Appl. Opt. 22, 535–540

Miles, R. B.; Connors J.; Markovitz E.; Howard P; Roth G. 1989: Instantaneous supersonic velocity profiles in an underexpanded sonic air jet by oxygen flow tagging. Phys. Fluids A 1, 389–393

Post, M. E. 1994: Two-dimensional velocity fields of vortex structures measured with two-color particle-imaging velocimetry. Ph.D. Dissertation. Cincinnati: University of Cincinnati

Ruess, D. L.; Adrian R. J.; Landreth C. C.; French D. T.; Fansler T. D. 1989: Instantaneous planar measurements of velocity and large-scale vorticity and strain rate in an engine using particle-image velocimetry. SAE Technical Paper 890616

Smallwood, G. J. 1992: A technique for two-color particle image velocimetry. Masters Thesis, Ottawa, Ontario, Canada: University of Ottawa

Warnet, M. P.; Edwards, R. V. 1990: New space domain processing technique for pulsed laser velocimetry. Appl. Opt. 29, 3399–3417

Yao, C. S.; Adrian, R. J. 1984: Orthogonal compression and 1-D analysis technique for measurement of 2-D particle displacements in pulsed laser velocimetry. Appl. Opt. 23, 1687–1689